Rate equation analysis of injection-locked quantum cascade lasers

Cheng Wang, Frédéric Grillot, Vassilios Kovanis, and Jacky Even

Related Articles

High beta lasing in micropillar cavities with adiabatic layer design
Appl. Phys. Lett. 102, 052114 (2013)

Portable optical-resolution photoacoustic microscopy with a pulsed laser diode excitation
Appl. Phys. Lett. 102, 053704 (2013)

Electro-optical and lasing properties of hybrid quantum dot/quantum well material system for reconfigurable photonic devices
Appl. Phys. Lett. 102, 053110 (2013)

Laser emissions from one-dimensional photonic crystal rings on silicon-dioxide
Appl. Phys. Lett. 102, 051103 (2013)

High-brightness tapered quantum cascade lasers
Appl. Phys. Lett. 102, 053503 (2013)

Additional information on J. Appl. Phys.

Rate equation analysis of injection-locked quantum cascade lasers

Cheng Wang,[1,a)] Frédéric Grillot,[2] Vassilios Kovanis,[3,4] and Jacky Even[1]

[1]*Université Européenne de Bretagne, INSA, CNRS FOTON, 20 avenue des buttes de Coesmes, 35708 Rennes, France*
[2]*Telecom Paristech, Ecole Nationale Supérieure des Télécommunications, CNRS LTCI, 46 rue Barrault, 75013 Paris, France*
[3]*Air Force Research Laboratory, 2241 Avionics Circle, Wright-Patterson AFB, Dayton, Ohio 45433, USA*
[4]*Electro Science Laboratory, The Ohio State University, 1320 Kinnear Road, Columbus, Ohio 43212, USA*

The modulation properties of optical injection-locked quantum cascade lasers (QCLs) are investigated theoretically via a simple low dimensional rate equation model. It is found that both strong injection level and positive optical frequency detuning increase the modulation bandwidth, while a large linewidth enhancement factor (LEF) contributes to the enhancement of the peak magnitude in the intensity modulation (IM) response. As opposed to conventional injection-locked interband lasers, it is demonstrated that no dip occurs in the QCL's IM response, which is beneficial for a series of broadband microwave photonic applications. Computations also show that the value of the LEF can critically modify both the locking and stability regions on the optical frequency detuning injection level map. © *2013 American Institute of Physics.*
[http://dx.doi.org/10.1063/1.4790883]

I. INTRODUCTION

Quantum cascade lasers (QCLs) have been of great interest technologically since the first demonstration by Faist *et al.* in 1994.[1] Due to the intersubband optical transitions, the spectra of QCLs range from mid-infrared down to terahertz,[2,3] which can be widely used in optical communications, high resolution spectroscopy, imaging, and remote sensing.[3] Indeed, due to the small carrier lifetime as compared to the photon lifetime, one particular feature of QCLs is the absence of free-running relaxation oscillations in the electrical modulation response. Thus, because of the short stimulated lifetime combined to the cascade of photons, QCLs lead to ultra-wide modulation bandwidth, which is highly desirable for free-space short-range communications.[4] Besides, the short non-radiative lifetime can suppress the relaxation oscillations resulting in an over-damped class A oscillator with carrier equilibrium completely restored after one photon roundtrip. Assuming a simplified set of rate equations, the modulation bandwidth was predicted to be as large as of 100 GHz.[4,5] Values up to terahertz were even theoretically calculated in intersubband semiconductor lasers based on a triple quantum well structure.[6,7] However, these values are lowered to tens of gigahertz when using a full rate equation approach taking into account the QCL periods as well as the ground level from which electrons leave the active region into the injector of the next stage.[8,9] Experimentally, Paiella *et al.* reported a QCL emitting at 8 μm with a 10 GHz modulation bandwidth and no relaxation oscillation resonance.[10]

Besides modulation bandwidths up to 13 GHz and 24 GHz have also been measured on terahertz QCLs using a test bench technique.[11,12]

Since the relaxation oscillation is responsible for the dynamic stability in the free-running laser, a slight external perturbation such as modulation, optical injection, or self-injection is enough to induce sustained pulsating intensities.[13] Optical injection-locking technique is known to be an attractive approach for improving the modulation characteristics of directly modulated interband semiconductor lasers.[14,15] Indeed, optical injection can be instrumental for increasing the modulation bandwidth, reducing the laser's chirp, and suppressing the mode hopping phenomenon as well as the relative intensity noise.[16–18] For instance, a record relaxation resonance frequency of 72 GHz associated with a broadband response of 44 GHz has been reported in an injection-locked quantum well distributed feedback (DFB) laser. Such a bandwidth enhancement corresponds to a 5.5 fold improvement when compared to the free-running case.[17] A theoretical study has recently reported the impacts of optical injection on the modulation properties of QCLs.[19] Numerical results have pointed out that injection-locked QCLs show no unstable regime in the locking map, while giant modulation bandwidths as large as 200 GHz can be reached with a 10 dB injection level ratio.

This paper aims to go a step beyond in examining the intensity modulation (IM) properties of injection-locked QCLs as well as the influences of injection strength, frequency detuning, and linewidth enhancement factor (LEF) with respect to both fast and slow carrier removal rates. Based on a second-order system model, the modulation transfer function of the injection-locked laser is obtained from a small signal analysis. Calculations show that the modulation bandwidth is enhanced by both increasing the injection strength and positive frequency detuning, while a large LEF enlarges the peak amplitude in the modulation response. It is also demonstrated that a large LEF value is favourable to the bandwidth enhancement with a fast carrier removal rate,

a)Electronic mail: cheng.wang@insa-rennes.fr.

while it is in the opposite trend with a slow carrier removal rate. Finally, in contrast to conventional injection-locked interband semiconductor lasers, our calculations point out that no dip occurs in the QCLs' IM response.

II. NUMERICAL MODEL DESCRIPTION

The classical equation describing the complex field of an injection-locked laser is as follows:[20,21]

$$\frac{dE(t)}{dt} = \frac{1}{2}\left(G - \frac{1}{\tau_P}\right)(1 + j\alpha_H)E(t) + k_c A_{inj} - j\Delta\omega_{inj}E(t), \quad (1)$$

where $E(t)$ is the slave laser's complex field, G is the gain, τ_P is the photon lifetime, A_{inj} is the injected field magnitude, α_H is the LEF, $\Delta\omega_{inj}$ is the frequency detuning defined as $\Delta\omega_{inj} = \omega_{master} - \omega_{slave}$, and k_c is the coupling rate of the master laser into the slave laser which is $k_c = c(1 - R)/(2n_r L\sqrt{R})$ with n_r the refractive index and L the cavity length. The complex rate equation (1) can be split into two coupled rate equations for the photon number and the phase, according to the relationship $E(t) = \sqrt{S(t)}\exp j\Delta\phi(t)$ with the phase difference $\Delta\phi = \phi_{slave} - \phi_{master}$. Along with the simplified carrier rate equation,[7] the rate equations for injection-locked QCLs are finally given by

$$\frac{dN_{up}}{dt} = \frac{I}{q} - \frac{N_{up}}{\tau_N} - G_0\Delta NS, \quad (2)$$

$$\frac{dN_{low}}{dt} = \frac{N_{up}}{\tau_N} + G_0\Delta NS - \frac{N_{low}}{\tau_R}, \quad (3)$$

$$\frac{dS}{dt} = (G_0\Delta N - 1/\tau_P)S + \beta\frac{N_{up}}{\tau_{sp}} + 2k_c\sqrt{S_{inj}S}\cos\Delta\phi, \quad (4)$$

$$\frac{d\Delta\phi}{dt} = \frac{\alpha_H}{2}(G_0\Delta N - 1/\tau_P) - \Delta\omega_{inj} - k_c\sqrt{\frac{S_{inj}}{S}}\sin\Delta\phi, \quad (5)$$

where N_{up} and N_{low} are the carrier numbers in the upper and lower subbands, respectively. In the model, the QCL is assumed to be composed of one period as in Ref. 7. The active region is based on the so-called three-quantum-well vertical transition design.[22–24] Fig. 1 illustrates the sketch of the carrier dynamics in the injection-locked QCL. The carriers are injected into the upper subband of the active region by resonant tunnelling, while the tunnelling time from the injector is ignored since it is extremely short (~ 0.2 ps).[1] Then, the carriers relax into the lower subband, from which these leave the active region. Neither the carrier absorption process nor the ground level in the active region is taken into
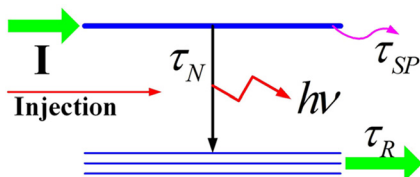

FIG. 1. Sketch of the simplified carrier dynamics model in injection-locked QCLs.

account in the simulations. The symbol τ_N denotes the carrier relaxation time from the upper subband, τ_R is the carrier removal time from the lower subband, τ_{sp} is the spontaneous emission lifetime, β is the spontaneous emission factor, and S_{inj} is the injected photon number. The linear gain $G = G_0\Delta N$ is proportional to $\Delta N = N_{up} - N_{low}$ as well as to the gain coefficient G_0, which corresponds to the differential gain multiplied by the group velocity. Although the approach used in this paper is simplified as compared to an actual QCL band structure, it is shown in the following that some preliminary insights regarding the high-speed properties of optically-injected QCLs can be extracted.

Neglecting the spontaneous term in Eq. (4) and setting the rate equations (2)–(5) to zero, the steady-state solution is obtained as follows:

$$S = \frac{k_c^2 S_{inj}}{\frac{1}{4}(G_0\Delta N - 1/\tau_p)^2 + \left(\frac{\alpha_H}{2}(G_0\Delta N - 1/\tau_p) - \Delta\omega_{inj}\right)^2}, \quad (6)$$

$$\Delta N = N_{up} - N_{low} = \frac{1}{G_0}\left(\frac{1}{\tau_p} - 2k_c\sqrt{\frac{S_{inj}}{S}}\cos\Delta\phi\right), \quad (7)$$

$$\Delta\phi = \sin^{-1}\left[\frac{-\Delta\omega_{inj}}{k_c\sqrt{1 + \alpha_H^2}}\sqrt{\frac{S}{S_{inj}}}\right] - \tan^{-1}\alpha_H. \quad (8)$$

It is noted that the carrier number in the lower subband is not impacted by the injection locking, which is $N_{low} = \tau_R I/q$ as in the free-running laser. In Eq. (7), ΔN is reduced by $2k_c\sqrt{S_{inj}/S}\cos\Delta\phi/G_0$ from the free running value $\Delta N_{fr} = 1/(G_0\tau_p)$.

In order to obtain the small-signal responses to a small current deviation I_1, the deviations of $N_{up}, N_{low}, S, \Delta\phi$ are defined as N_{up1}, N_{low1}, S_1, and $\Delta\phi_1$, respectively. Then, the differential rate equation can be derived from the rate equations (2)–(5) via a standard small-signal analysis as follows:

$$\begin{bmatrix} \gamma_{11} + j\omega & -\gamma_{12} & -\gamma_{13} & 0 \\ -\gamma_{21} & \gamma_{22} + j\omega & -\gamma_{23} & 0 \\ -\gamma_{31} & -\gamma_{32} & \gamma_{33} + j\omega & -\gamma_{34} \\ -\gamma_{41} & -\gamma_{42} & -\gamma_{43} & \gamma_{44} + j\omega \end{bmatrix}\begin{bmatrix} N_{up1} \\ N_{low1} \\ S_1 \\ \Delta\phi_1 \end{bmatrix} = \frac{I_1}{q}\begin{bmatrix} 1 \\ 0 \\ 0 \\ 0 \end{bmatrix}, \quad (9)$$

with

$$\gamma_{11} = G_0 S + 1/\tau_N; \quad \gamma_{12} = G_0 S; \quad \gamma_{13} = -G_0\Delta N;$$
$$\gamma_{21} = G_0 S + 1/\tau_N; \quad \gamma_{22} = G_0 S + 1/\tau_R; \quad \gamma_{23} = G_0\Delta N;$$
$$\gamma_{31} = G_0 S + \beta/\tau_{sp}; \quad \gamma_{32} = -G_0 S;$$
$$\gamma_{33} = \frac{1}{\tau_P} - G_0\Delta N - k_c\cos\Delta\phi\sqrt{\frac{S_{inj}}{S}};$$
$$\gamma_{34} = -2k_c\sin\Delta\phi\sqrt{S_{inj}S}; \quad \gamma_{41} = \frac{\alpha_H}{2}G_0; \quad (10)$$
$$\gamma_{42} = -\frac{\alpha_H}{2}G_0; \quad \gamma_{43} = \frac{k_c\sin\Delta\phi}{2S}\sqrt{\frac{S_{inj}}{S}};$$
$$\gamma_{44} = k_c\cos\Delta\phi\sqrt{\frac{S_{inj}}{S}}.$$

Then, the modulation transfer function can be extracted as follows:

$$H(w) = \frac{S_1(\omega)/J_1(\omega)}{S_1(0)/\Delta J_1(0)} = \frac{p_1 p_2 p_3 p_4}{z_1 z_2} \frac{(j\omega - z_1)(j\omega - z_2)}{\prod\limits_{i=1}^{4}(j\omega - p_i)}, \quad (11)$$

where z_1 and z_2 are zeros, which are expressed as $z_1 = k_c \sqrt{S_{inj}/S}(\alpha_H \sin\Delta\phi - \cos\Delta\phi)$; $z_2 = 1/\tau_N - 1/\tau_R$, respectively. Parameter z_1 is mainly determined by the injection condition while z_2 is related to the difference between the carrier relaxation and carrier removal rates. The denominator of Eq. (11) represents a polynomial function whose expression comes from the determinant of the coefficient matrix in Eq. (9). It is noted that the analytical expressions of the poles p_1-p_4 are too complicated to be extracted due to the complexity of the transfer function.

III. RESULTS AND DISCUSSIONS

In the simulations, the lasing wavelength is $\lambda = 8.0 \, \mu m$, the gain coefficient is $G_0 = 2.5 \times 10^5 \, s^{-1}$, the carrier relaxation time is $\tau_N = 1.5 \, ps$ and the refractive index is $n_r = 3.27$. These parameters follow those reported on devices from Ref. 25. Other parameters[9] are $\tau_{sp} = 7 \, ns$, $\beta = 10^{-4}$, and $R = 0.29$. The bias current is fixed at $I = 1.2 I_{th}$. Although the typical cavity length of QCLs is in the order of millimetre,[8,25] shorter cavity is usually desirable for higher modulation bandwidth. In consequence, the cavity length chosen in our simulation is set down to $L = 0.15 \, mm$ as in Ref. 5, resulting in a photon lifetime of $\tau_P = 1 \, ps$.

First, we studied the injection-locking map of the QCLs. The boundaries derived from Eqs. (7) and (8) show that the variation of the phase across the locking range varies from $\cot^{-1}\alpha_H$ at the negative frequency detuning edge to $-\pi/2$ at the positive frequency detuning edge.[26] Then, the locking regime can be obtained by rearranging Eq. (8)

$$\Delta\omega_{inj} = -k_c\sqrt{1 + \alpha_H^2}\sqrt{S_{inj}/S}\sin(\Delta\phi + \tan^{-1}\alpha_H). \quad (12)$$

Fig. 2 shows the locking map as functions of the detuning frequency and the injection ratio $R_{inj} = S_{inj}/S_{FE}$, where S_{FE} is the photon number of the free-running laser. Although
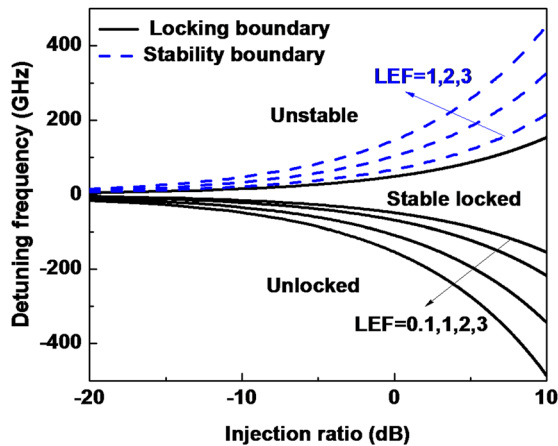

FIG. 2. Optical injection-locking diagram as function of the detuning frequency and the injection ratio. Solid lines are the locking regime boundaries; the negative detuning frequency boundaries are calculated with LEF = 0.1, 1, 2, and 3, respectively; dashed line is the stability boundary.

QCLs theoretically exhibit a near-zero subthreshold LEF because of the homogeneously broadened gain medium, recent experiments have shown that the above-threshold LEF of QCLs can actually deviate from the subthreshold values in the range from 0 to about 2.5.[25,27–29] To this end, calculations in this paper are conducted for LEF values of 0.1, 1, 2, and 3. The boundaries (solid line) between the locked and unlocked regimes are obtained from Eqs. (7), (8), and (12). As for interband lasers, the locking range increases with the injection ratio. Calculations also show that the LEF mainly influences the locking diagram especially at the negative frequency detuning boundary, which shifts down at larger LEFs. The stability boundary can be obtained from the pole extraction of the IM response (see Eq. (11)) via a stability analysis,[16] which is indicated by dashed lines in Fig. 2. The stable regime enlarges with higher LEF values. Interestingly, for LEF = 0.1, the system is found always stable when the injection ratio gets larger than 0.05 (the boundary for $R_{inj} < 0.05$ is not shown since it overlaps other plots). Unlike the traditional locking map of interband lasers, simulations point out that in the case of injection-locked QCLs, there is no unstable regime (Period one, Period doubling, chaos) in the locking range as already reported in Ref. 19, This effect is attributed to the ultrafast carrier lifetime of the upper laser state. However, at this stage, we believe that this prediction has to be supported via a deeper non-linear dynamics analysis conducted on a full rate equation model.

In what follows, based on the analysis of the stable locking regime, the IM properties of optically-injected QCLs are investigated both for fast and slow carrier removal rates. According to Ref. 7, for fast carrier removal rates, the free-running QCL IM response does not exhibit a peak while it pops-up at slow carrier removal rates. Calculations also show that this peak is not due to the carrier-photon relaxation resonance as for interband lasers, but to the zero occurring in the modulation transfer function.

A. IM response with fast carrier removal rate

The carrier removal time is set to be $\tau_R = 0.21 \, ps$. Figs. 3(a)–3(c) show the optical injection-locking IM response of the QCLs as a function of the injection ratio R_{inj}, frequency detuning Δf, and LEF, respectively. As depicted in Fig. 3(a) at zero detuning with LEF = 1, the bandwidth f_{3dB} increases with the injection ratio, and the modulation response remains relatively flat with no peak. At $R_{inj} = 10 \, dB$, the modulation bandwidth (163 GHz) is more than 3-fold enhanced as compared to the free-running one (51 GHz). In comparison, in the case of injection-locked interband lasers, there is an optimum injection strength, above which the modulation bandwidth starts decreasing.[18]

Since the IM response shape can be analyzed through the Bode plot, poles and zeros as well as the 3 dB bandwidths have been determined for Fig. 3(a), and the corresponding values are listed in Table I. Because $|z_1|$, $|p_1|$, and $|p_2|$ are much smaller than the other poles and zeros, those play a dominant role in the IM response.[7] As seen in Fig. 3(a), the initial slope of the modulation response is 0 dB/decade. When the modulation frequency exceeds the zero value $|z_1|$,
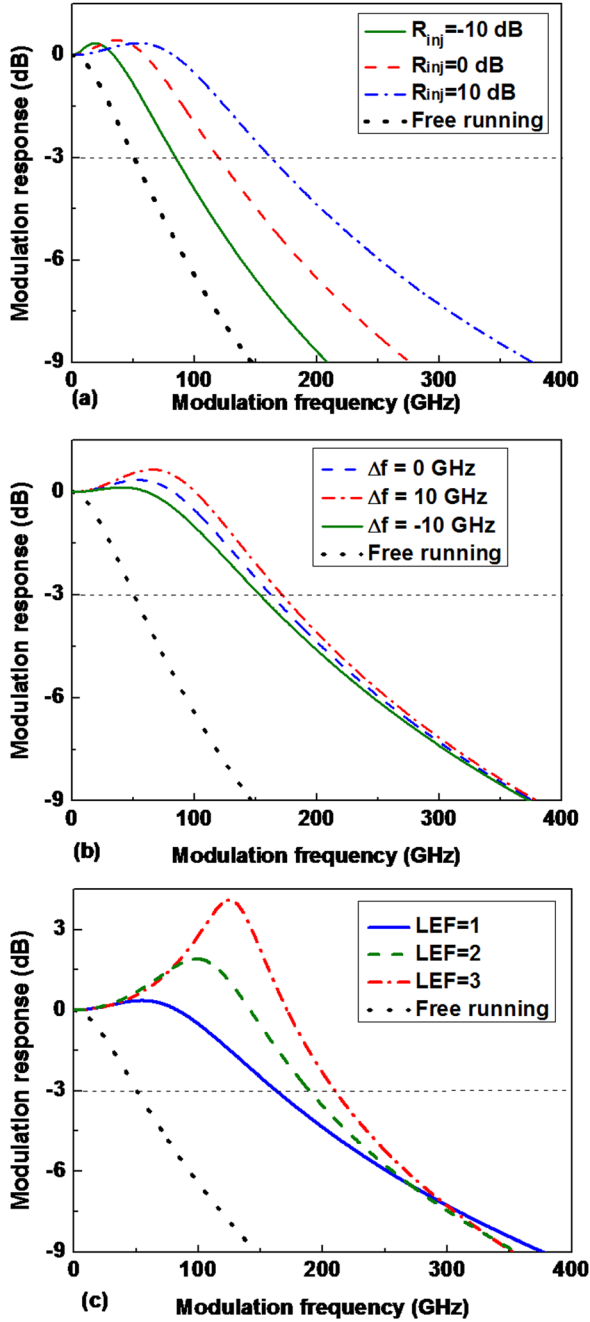
FIG. 3. IM response of optical injection-locked QCLs for fast carrier removal rate ($\tau_R = 0.21$ ps) as a function of (a) injection ratio R_{inj} at zero detuning with LEF = 1, (b) detuning frequency Δf at $R_{inj} = 10$ dB with LEF = 1, and (c) LEF at zero detuning with $R_{inj} = 10$ dB.

TABLE I. Poles, zeros, and bandwidths (GHz) for Fig. 3(a).

R_{inj} (dB)	p_1	p_2	p_3	p_4	z_1	z_2	f_{3dB}
Free		−35.3	−93.2	−777.9		−651.8	50.9
−10	−24.3	−47.5	−87.5	−793.6	−16.7	−651.8	84.9
0	−50.2 ± j35.9		−105.1	−825.4	−39.8	−651.8	120
10	−64.9 ± j64.6		−173.5	−947.9	−81.0	−651.8	163

the slope of the Bode diagram starts increasing until the frequency reaches the pole $|p_1|$. Because $|p_1|$ is close to $|z_1|$, only a relatively small peak is observed in the modulation response. At larger modulation frequencies, the break-up

point, which is due to the pole $|p_2|$, induces a decrease of the Bode plot with a slope of -20 dB/decade. This dominant pole $|p_2|$ can be used to evaluate the 3 dB bandwidth such as[7]

$$f_{3dB} \approx \sqrt{3}|p_2|. \tag{13}$$

Typically, modulation responses of injection-locked interband lasers exhibit a linear response at negative detuning conditions without resonance peak. At zero detuning, the laser is characterized by a broadband and flat response, while for positive frequency detuning, the modulation response shows an even higher resonance frequency associated with a sharp peak and a large pre-resonance frequency dip.[16–18] The enhanced resonance frequency originates from the interference between the locked field and the shifted cavity-resonance field,[16] while the sharp peak is due to the small damping factor of the oscillation. The pre-resonance frequency dip significantly limits the 3 dB bandwidth and constitutes one of the major limitations of injection-locked interband lasers. In the case of conventional lasers with quantum well materials, the modulation transfer function holds a pair of complex conjugate poles, one real pole and one zero. In such way, the dip results from the smaller real pole value as compared to the zero value.[17] As the modulation bandwidth can be enhanced with a high injection ratio, the impacts of the frequency detuning on injection-locked QCLs are studied under strong optical injection of $R_{inj} = 10$ dB assuming LEF = 1. Fig. 3(b) shows that the positive frequency detuning case enhances the modulation bandwidths, which are 154 GHz, 163 GHz, and 172 GHz for detuning frequencies of -10 GHz, 0 GHz, and 10 GHz, respectively (see Table II). In contrast to interband lasers, it is noted that injection locked QCLs do not exhibit a dip in the modulation response, especially at positive frequency detuning. From Table II, the absence of the pre-resonance dip can be attributed to the fact that the zero $|z_1|$ is smaller than all the poles. Fig. 3(c) presents the influences of the LEF on the modulation response at zero detuning with an injection ratio of $R_{inj} = 10$ dB. Calculations point out that a large LEF is more favourable since the modulation bandwidth is enhanced from 163 GHz (LEF = 1) up to 210 GHz (LEF = 3). Let us stress that because of the pole p_2, which becomes closer to the imaginary axis, a large LEF value increases the peak amplitude and results in an under-damped modulation response.

B. IM response with slow carrier removal rate

The carrier removal time is set to be $\tau_R = 1.2$ ps. Figs. 4(a)–4(c) illustrate the optical injection-locking IM response of the QCLs as a function of the injection ratio R_{inj},

TABLE II. Poles, zeros, and bandwidths (GHz) for Fig. 3(b).

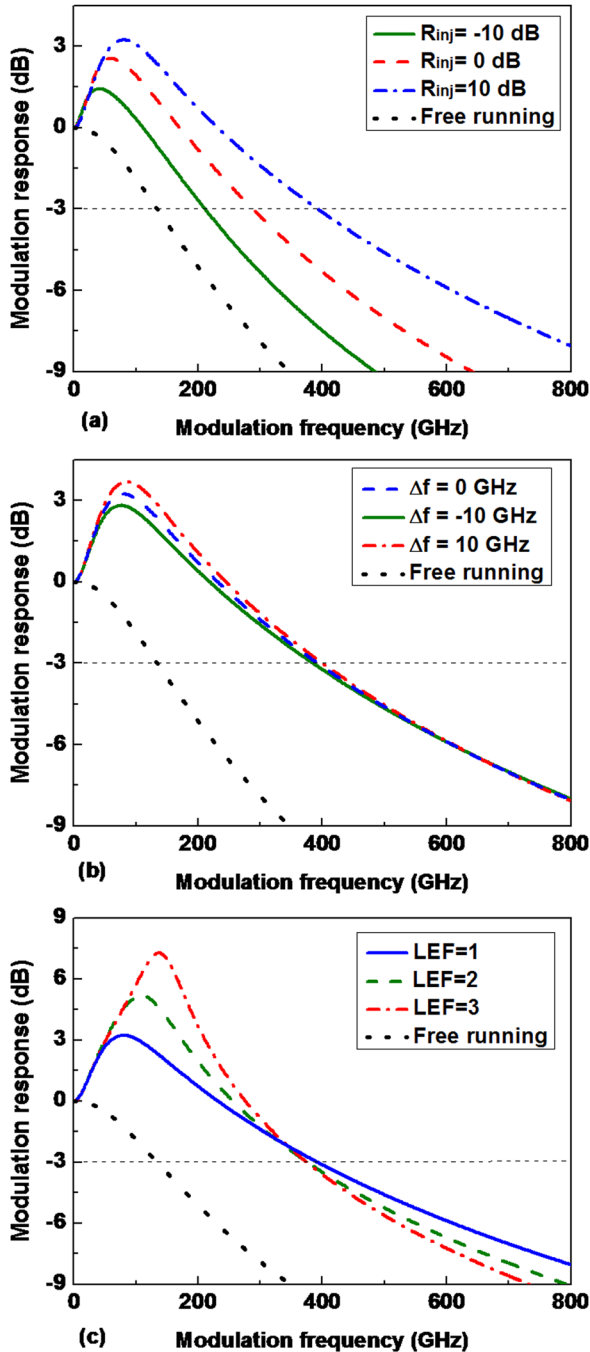| Δf	p_1	p_2	p_3	p_4	z_1	z_2	F_{3dB}
−10	−69.2 ± j53.7		−178.8	−974.6	−76.0	−651.8	154
0	−64.9 ± j64.6		−173.5	−947.9	−81.0	−651.8	163
10	−60.1 ± j74.2		−168.3	−922.6	−85.4	−651.8	172

FIG. 4. IM response of optical injection-locked QCLs for slow carrier removal rate ($\tau_R = 1.2$ ps) as a function of (a) injection ratio R_{inj} at zero detuning with LEF = 1, (b) detuning frequency Δf at $R_{inj} = 10$ dB with LEF = 1, and (c) LEF at zero detuning with $R_{inj} = 10$ dB.

TABLE III. Poles, zeros, and bandwidths (GHz) for Fig. 4(a).

R_{inj} (dB)	p_1	p_2	p_3	p_4	z_1	z_2	f_{3dB}
Free		-26.5	$-127.3 \pm j26.0$			-26.5	135
-10	$-26.3 \pm j6.1$		$-137.9 \pm j20.0$		-16.7	-26.5	212
0	$-44.0 \pm j25.3$		-106.9	-212.1	-39.9	-26.5	289
10	$-69.9 \pm j57.2$		-71.6	-418.0	-81.3	-26.5	393

frequency detuning, and LEF, respectively. The poles, zeroes, and calculated 3 dB bandwidth related to Fig. 4(a) are listed in Table III. In Fig. 4(a) at zero detuning with

TABLE IV. Poles, zeros, and bandwidths (GHz) for Fig. 4(b).

Δf	p_1	p_2	p_3	p_4	z_1	z_2	f_{3dB}
-10	$-71.8 \pm j46.0$		-71.5	-455.1	-76.3	-26.5	385
0	$-69.9 \pm j57.2$		-71.6	-418.0	-81.3	-26.5	393
10	$-67.3 \pm j67.6$		-72.0	-382.4	-85.7	-26.5	400

LEF = 1, both the peak magnitude and the bandwidth increase with the injection ratio. Under strong optical injection ($R_{inj} = 10$ dB), the bandwidth (393 GHz) is about 3 times larger as compared to the free-running case (135 GHz). This strong enhancement is the consequence of the slow carrier removal rate making the zero $|z_2|$ smaller than the other poles. Thus, $|z_2|$ when associated with the small zero $|z_1|$ leads to a peak arising in the IM response.

Fig. 4(b) depicts the effect of the frequency detuning on the modulation response for an injection ratio of $R_{inj} = 10$ dB assuming LEF = 1. Similarly to the fast carrier removal rate case, the 3 dB bandwidth is enhanced at positive frequency detuning region. As illustrated in Table IV, for detuning frequencies of -10 GHz, 0 GHz, and 10 GHz, the modulation bandwidths are 385 GHz, 393 GHz, and 400 GHz, respectively. Besides, the peak amplitude increases with the detuning frequency as well. Calculations demonstrate one more time the absence of the pre-resonance frequency dip in the modulation response. Similarly to the fast carrier removal rate case, Fig. 4(c) obtained under zero detuning and with $R_{inj} = 10$ dB shows that the peak amplitude is sensitive to the LEF. This effect is also due to the pole p_2, which becomes closer to the imaginary axis in the pole-zero plot. On the contrary, let us note that a large LEF combined with a slow carrier removal rate reduces the 3 dB bandwidth from 393 GHz (LEF = 1) to 375 GHz (LEF = 3).

As previously mentioned, in contrast to interband lasers,[18] one of the key features of injection-locked QCLs is the absence of the dip in the IM response no matter what the carrier removal rate case. These results indicate that the dip, which is one of the major drawbacks limiting the 3 dB bandwidth of injection-locked interband lasers, does not occur with QCLs. This difference is attributed to the ultrafast carrier dynamics resulting from the intersubband transitions in QCLs. The elimination of the dip is highly desirable to match the broadband requirements of high-speed communication systems as well as for free-space short range communications.

IV. CONCLUSIONS

Based on a simplified rate equation model, the modulation properties of optical injection-locked QCLs have been investigated taking into account the influences of the LEF and the carrier removal rate. These preliminary results are of prime importance for the improvements of the modulation properties of QCLs. Calculations show that the modulation bandwidth increases both with positive frequency detuning and the injection strength. In the latter, the modulation bandwidth for the laser with a 10 dB injection ratio can be up to 3 fold improved in comparison with the free-running case. The

magnitude of the peak in the IM response is sensitive to the LEF and gets enlarged with large LEF values. In comparison with conventional injection-locked interband semiconductor lasers, calculations point out that no dip occurs in the QCLs' IM response. Although the calculations demonstrate no unstable regime in the locking range, we believe that this interesting finding has to be confirmed via a systematic nonlinear dynamics analysis. To this end, future work will consider an enhanced rate equation model by taking into account the ground level from which electrons leave the active region into the injector of the next stage, gain compression as well as QCL periods, so as to emphasize the effects of the enhanced photon number in the laser cavity. Investigation of the optically-injected QCL spectral properties will be also in the context for future high performance oscillators, like low noise tunable photonic oscillators, in wavelengths from 3 to 5 μm, which can be enable multiple radio frequency photonics applications. Finally, future work will also take into account the impacts of the key relaxation time from the upper laser state to the lower laser state, which is known to have significant influences on the modulation response of free-running QCLs.

ACKNOWLEDGMENTS

[1]J. Faist, F. Capasso, D. L. Sivco, C. Sirtori, A. L. Hutchinson, and A. Y. Cho, Science **264**, 553 (1994).

[2]C. Gmachl, F. Capasso, D. L. Sivco, and A. Y. Cho, Rep. Prog. Phys. **64**, 1533 (2001).

[3]S. Kumar, IEEE J. Sel. Top. Quantum Electron. **17**, 38 (2011).

[4]N. Mustafa, L. Pesquera, C. Y. L. Cheung, and K. A. Shore, IEEE Photon. Technol. Lett. **11**, 527 (1999).

[5]C. Y. L. Cheung, P. S. Spencer, and K. A. Shore, IEEE Proc.: Optoelectron. **144**, 44 (1997).

[6]K. Donovan, P. Harrison, and R. W. Kelsall, J. Appl. Phys. **89**, 3084 (2001).

[7]M. K. Haldar, IEEE J. Quantum Electron. **41**, 1349 (2005).

[8]F. Rana and R. J. Ram, Phys. Rev. B **65**, 125313 (2002).

[9]Y. Petitjean, F. Destic, J. C. Mollier, and C. Sirtori, IEEE J. Quantum Electron. **17**, 22 (2011).

[10]R. Paiella, R. Martini, F. Capasso, and C. Gmachl, Appl. Phys. Lett. **79**, 2526 (2001).

[11]S. Barbieri, W. Maineult, S. S. Dhillon, C. Sirtori, and J. Alton, Appl. Phys. Lett. **91**, 143510 (2007).

[12]W. Maineult, L. Ding, P. Gellie, P. Filloux, and C. Sirtori, Appl. Phys. Lett. **96**, 021108 (2010).

[13]T. B. Simpson, J. M. Liu, M. Almulla, N. Usechak, and V. Kovanis, in *2012 IEEE International on Frequency Control Symposium*, Baltimore, USA (2012), pp. 1–5.

[14]V. Kovanis, T. Erneux, and A. Gavrielides, Opt. Commun. **159**, 177 (1999).

[15]A. Gavrielides, V. Kovanis, and T. Erneux, Opt. Commun. **136**, 253 (1997).

[16]A. Murakami, K. Kawashima, and K. Atsuki, IEEE J. Quantum Electron. **39**, 1196 (2003).

[17]E. K. Lau, H. K. Sung, and M. C. Wu, IEEE J. Quantum Electron. **44**, 90 (2008).

[18]N. A. Naderi, M. Pochet, F. Grillot, N. B. Terry, V. Kovanis, and L. K. Lester, IEEE J. Sel. Top. Quantum Electron. **15**, 1349 (2009).

[19]B. Meng and Q. J. Wang, Opt. Express **20**, 1450 (2012).

[20]R. Lang, IEEE J. Quantum Electron. **QE-18**, 976 (1982).

[21]T. Erneux, V. Kovanis, A. Gavrielides, and P. M. Alsing, Phys. Rev. A. **53**, 4372 (1996).

[22]J. Faist, F. Capasso, C. Sirtori, D. L. Sivco, J. N. Baillargeon, A. L. Hutchinson, S. N. G. Chu, and A. Y. Cho, Appl. Phys. Lett. **68**, 3680 (1996).

[23]C. Sirtori, J. Faist, F. Capasso, D. L. Sivco, A. L. Hutchinson, and A. Y. Cho, Appl. Phys. Lett. **66**, 3242 (1995).

[24]C. Gmachl, A. Tredicucci, F. Capasso, A. L. Hutchinson, D. L. Sivco, J. N. Baillargeon, and A. Y. Cho, Appl. Phys. Lett. **72**, 3130 (1998).

[25]F. Capasso, R. Paiella, R. Martini, R. Colombelli, C. Gmachl, and T. L. Myers, IEEE J. Quantum Electron. **38**, 511 (2002).

[26]F. Mogensen, H. Olesen, and G. Jacobsen, IEEE J. Quantum Electron. **QE-21**, 784 (1985).

[27]R. P. Green, J. H. Xu, L. Mahler, A. Tredicucci, and F. Beltram, Appl. Phys. Lett. **92**, 071106 (2008).

[28]T. Aellen, R. Maulini, R. Terazzi, N. Hoyler, M. Giovannini, and J. Faist, Appl. Phys. Lett. **89**, 091121 (2006).

[29]J. V. Staden, T. Gensty, and W. Elsaber, Opt. Lett. **31**, 2574–2576 (2006).